Cryogenic Composite Tank Design for Next Generation Launch Technology

Galib H. Abumeri[1]
QSS Group Inc., Cleveland, Ohio, 44135

Daniel N. Kosareo[2]
Zin Technologies Inc., Brook Park, Ohio, 44142

and

Joseph M. Roche[3]
NASA Glenn Research Center, Cleveland, Ohio, 44135

The structural performance of liquid hydrogen tanks made from composites is investigated. A computational method that judiciously combines structural analysis, composite mechanics, progressive fracture algorithm to evaluate damage tolerance, durability, and fatigue and fracture is described. A tank design concept is introduced and evaluated. The composite tank is internally stiffened by incorporating additional stacks of laminates along its length to alternate rows of finite elements. The robustness of the proposed design concept is assessed by damage progression analysis. Damage initiates in the composite at an internal pressure that is nearly two times the design pressure. From the point of damage initiation, the designed tank can tolerate an increase in internal pressure that is nearly three and a half times the design pressure. Low cycle fatigue analysis is also performed to determine the effect of pressurization and de-pressurization on the structural integrity of the tank. Results show that the tank can sustain at least a 100 cycles before any ply failure take place.

Nomenclature

A_ℓ	=	laminate extensional stiffness matrix
a	=	first parameter for degrading fiber or matrix properties
B_ℓ	=	laminate bending stretching coupling matrix
b	=	second parameter for degrading fiber or matrix properties
D_ℓ	=	laminate flexural stiffness matrix
C	=	damping matrix
F	=	external forces vector
K	=	stiffness matrix
M	=	mass matrix
M_ℓ	=	nodal bending moments
N_ℓ	=	nodal in-plane forces
ε_ℓ	=	nodal in-plane strain
κ_ℓ	=	nodal curvatures
t	=	time
$\mathbf{u}$	=	nodal displacement vector
$\dot{\mathbf{u}}$	=	nodal velocity vector
$\ddot{\mathbf{u}}$	=	nodal acceleration vector

[1] Aerospace Engineer, QSS Group Inc., 21000 Brookpark Rd /MS GES-QSS, Cleveland, OH, 44135
[2] Senior Project Engineer, Zin Technologies Inc., 3000 Aerospace Parkway/MS GES-ZIN, Brook Park, OH, 44142
[3] Chief Systems Engineering Services & Advanced Concepts Branch, NASA Glenn Research Center, 21000 Brookpark Rd /MS 86-15, Cleveland, OH, 44135

I. Introduction

THE Next Generation Launch Technology (NGLT) program, under NASA sponsorship, was mainly aimed to enable NASA to expand the scientific and human exploration of space. Other goals of the program were to enable the U.S. to maintain and grow its share in the commercial launch vehicle market, and provide support to the country's national security needs. In an effort to address a range of mission needs, the Andrews Gryphon booster architecture concept was developed. Gryphon is a horizontal takeoff horizontal landing (HTHL) reusable launch vehicle (RLV). It uses an air collection enrichment system named ACES, which has the function of collecting and cooling oxygen during the subsonic segment of the flight. Generating liquid oxygen during flight reduces the gross takeoff weight and maximizes the payload to orbit. The 1st stage Gryphon concept is designed to house ACES and transport a 2nd stage to an altitude of 180,000 ft. It is estimated that a total of eight large military engines and four SSME LOX (liquid oxygen)/LH2 (liquid hydrogen) rocket engines would be required to propel the 1st stage.

The technology of advanced fiber composites has progressed to the point that these composites are prime contenders for various aerospace applications. Their outstanding mechanical properties are very attractive to the aerospace industry, especially the ratios of high strength to weight and high stiffness to density. They also possess excellent fatigue strength and the ability to resist corrosion and impact. Tanks made from advanced composites are considered for storing the propellant in the 1st stage Gryphon booster as shown in Fig. 1. Designing with composites poses challenges that include hermiticity, durability, and life. Additional challenges result from actual operating loads and environmental conditions. The difficulties in design are further compounded by inherent uncertainties in the thermo-mechanical material properties for fiber and matrix, structural geometry (shape), fabrication process variables, and loading. A computational simulation methodology with a wide-ranging capability is essential for an effective design. The methodology must include: (1) general purpose finite element structural analysis, (2) micromechanics based composite mechanics, (3) progressive fracture algorithm used to evaluate damage tolerance, durability, and fatigue and fracture, and (4) an efficient probabilistic algorithm for evaluating the reliability. The scope of this paper is focused on the deterministic conceptual design approach for cryogenic tank applications. Future efforts will address the effect of uncertainties on the robustness of the design of cryogenic composite tanks.

The objective of this investigation is to assess the structural performance of the forward LH2 tank of the Gryphon vehicle. Methods and codes for simulating the behavior and response of composite material and structure in the application of a stiffened LH2 storage tank are described. It will be shown that the judicious combination of well established micro-mechanics theory, finite element analysis, damage tracking, and damage progression methods are sufficient to evaluate the durability of LH2 composite tanks. The robustness of the proposed tank design is evaluated by damage progression to assess the following: (1) when, where, and why damage is occurring, (2) when, where, and why failure is occurring, and (3) what can be done to delay damage initiation and failure. The stiffness of the composite tank includes a metallic liner, but the sealing capability of the liner is not addressed in the work presented in this paper.

The paper first explains the stiffened LH2 composite tank design concept. It is followed by a description of the composite material system (carbon fiber and a modified epoxy matrix with a thermoplastic phase for toughness). Then a brief overview of the GENOA computational software system used in assessing the structural performance of the tank is provided. Subsequently, results obtained from displacement and stress analysis, durability assessment, and low cycle fatigue evaluation are discussed.

II. Stiffened Composite Tank Design Concept

The stiffened LH2 composite tank design concept is described in this section. Shell structures are in general very efficient structural components for resisting combined thermo-mechanical loading conditions. The tank is made up of a cylindrical shell section and two ellipsoidal end caps. The ellipsoidal end caps are used to improve the storage capacity and packing efficiency of the tank. The length and diameter of the cylindrical sections are, 63 and 26 ft, respectively. The diameter of the ellipsoidal end cap is 26 ft and the height is 9.1 ft. The overall length of the tank equals 81.2 ft. The finite element model developed specifically for the structural evaluation of the composite tank is shown in Fig. 2-a. The tank is modeled with 664 three dimensional four noded shell elements with six degrees of freedom per node (three translations and three rotations). Cylindrical shells use composites effectively because of the ability to implement numerous fiber orientation patterns and constituent material properties.

Multiple ply schedules are used in various regions of the tank to provide the required stiffness to sustain the thermo-mechanical loading to which the tank is subjected. A ply schedule is basically a group of plies that require the following definitions: (1) thickness, (2) fiber orientation, (3) use and cure temperatures, and (4) material

selection, which include: fiber type, matrix type, and fiber volume ratio. The association of a ply with a particular material provides the designer the flexibility to tailor the stiffness of the structure as needed. As depicted in the tank's cross-sectional view in Fig. 2-b, the tank is stiffened by applying patches or additional stacks of plies at different locations in the tank. To prevent propellant leakage, an aluminum sheet (0.005" thick) is used as a liner. The composite is built around the liner with a bonding material to act as a galvanic barrier between the aluminum and the carbon fibers. Schedule 1 is made up of 10 plies while schedule 2 is made up of 20 plies (equivalent to two stacks of schedule 1). Ply schedules 1 and 2 are applied to alternating nodal lines along the length of the tank body (cylindrical section) as shown in Fig. 2-c. The implementation of ply schedule 2 provides an increase in stiffness and strength with minimum increase in weight. Ply schedule 2 is also applied to the center region of the end caps while the remaining end cap is made up with ply schedule 3. The latter ply schedule is made with 10 plies. The total thickness of ply schedule 1 and 3 is 0.1". The thickness of ply schedule 2 (stiffening patch) is 0.2". The total surface area of the tank is estimated be around 6,835 ft^2. The structural material volume of the composite (including the liner) is estimated around 181,831 in^3. The weight of the composite tank (empty) including the aluminum liner is estimated at 10,450 lb. The tank liquid hydrogen storage capacity (including the two elliptical caps) is calculated to be around 168,110 lb. That yields a total weight of 178,560 lb. When the tank is filled with liquid hydrogen (LH2), the temperature inside the tank drops to about -423 °F under a design internal pressure of 30 psi. Details of the composite material selection and definition of ply schedules are discussed in the next section.

III. Composite Material Characterization and Details of Ply Schedules

Polymer matrix composite materials are considered in cryogenic tank applications to replace traditional metallic materials. The IM7 fiber selected for the present study is a high strength, intermediate modulus, and continuous carbon fiber in a modified toughened epoxy 977-2 matrix. The fiber and matrix thermo-mechanical properties are tabulated in Table 1 and are derived from a laminate coupon stiffness test at cryogenic temperatures of -423 °F (see references 1, 2, and 3). Table 2 shows the layup details of the various ply schedules that are used in the tank design. The main idea here is to stiffen the tank by running along its length in an alternating fashion stacks of composites that are thicker than the one used in the rest of the structures. Such a configuration provides the necessary stiffness to resist the thermo-mechanical loading without a large increase in the tank weight. As shown in Table 2, the first and third ply schedules consist of 10 (0.01") plies but have different ply layup orientation and fiber volume ratio. Ply schedule 3 is used (as detailed in Fig. 2) for the two end cap regions. The use of higher fiber volume ratio for ply schedule 3 and the specified ply orientation provide additional laminate strength and increased stiffness to delay damage initiation in the end cap and shift the damage to the tank body, where it is easier to monitor and repair. Note that damage initiation is defined as the state when one or more plies have failed. The center of the end cap uses ply schedule 2 with 20 (0.01") plies to stiffen the center region to avoid premature damage initiation. The composite properties based on 60% and 65% fiber volume ratios are summarized in Table 3. The use of a 65% fiber volume ratio in ply schedule 3 (end cap regions) contributed directly to an increase in modulus and strength up to 8%. Although the fiber plays a key role in determining the overall composite properties, the matrix properties significantly affects the strength and stiffness of the composite. The fiber volume ratio selection process must take into account the application and the design requirements. A fiber volume ratio ranging from 50% to 65% is commonly used in polymer matrix composites.

IV. Description of Methodology

This section provides a brief description of the methodology used in the structural finite element, composite mechanics, and damage progression of the LH2 composite tank.

A. Structural Analysis

The general purpose structural finite element performs thermo-structural analyses static, dynamic, and various aspects of nonlinear analyses. The governing equation for general finite element structural analysis in matrix form is expressed:

$$[M]\{\ddot{u}\}+[C]\{\dot{u}\}+[K]\{u\}=\{F(t)\} \qquad (1)$$

The symbols in equation (1) are as follows: M is the mass matrix, C is the damping matrix, and K is the stiffness matrix of the structure or structural component; $\ddot{u}$, $\dot{u}$, and u are the nodal acceleration, velocity, and displacement, respectively. F is a combination of all external forces applied to the structure. Equation (1) is applicable to static, dynamic, impact, etc. It is applicable as well to temperature, moisture, time, and other material

nonlinearities. Various dependencies and nonlinearities are effectively evaluated by linear incrementation which is usually referred to as Up-dated Lagrangian. The tank structural analysis is carried out using the structural analysis software GENOA (Ref. 4). For more complete details on the theoretical background, see Ref. 4.

B. Composite Mechanics

The composite mechanics governing behavior is described by the following matrix equation:

$$\begin{Bmatrix} N_l \\ M_l \end{Bmatrix} = \begin{bmatrix} A_l & B_l \\ B_l^T & D_l \end{bmatrix} \begin{Bmatrix} \varepsilon_l \\ \kappa_l \end{Bmatrix} \qquad (2)$$

Equation (2) is referred to as the laminate Force-Deformation relationships. The notation in Eq. (2) is as follows: N_ℓ and M_ℓ are nodal in-plane forces and bending moments, respectively. ε_ℓ and κ_ℓ are nodal reference in-plane strains and curvatures, respectively. Aℓ, Bℓ, and Dℓ are the laminate in-plane (axial), coupling and bending (flexural) stiffness of the laminate, respectively. The B_l^T matrix is the transpose of the Bℓ matrix. Aℓ, Bℓ and Dℓ are generated by composite micromechanics and lamina configuration. Environmental effects and some fabrication variables are included through the laminate configuration. For more details, see reference 5, which is the computer code for composite mechanics identified as ICAN for Integrated Composite ANalyzer.

C. Durability Analysis

The robustness of a particular design must be evaluated using damage progressive analysis to assess the load carrying ability of the structure. Damage in composite structures needs to be quantified at the following segments: (1) initiation, (2) stable propagation up to a critical amount, and (3) rapid propagation up to catastrophic failure. Damage initiation is defined as the state where one or more plies have failed. The structural analysis software GENOA (Ref. 4) is capable of performing damage progression analysis of structures that are made with polymer, metal, and ceramic matrix composites. GENOA combines judiciously the following disciplines: (1) composite mechanics, (2) finite element analysis, (3) material degradation, and (4) damage tracking/accumulation algorithm (Ref. 6). Loadings spectrum available in GENOA includes: static, low/high cycle fatigue, harmonic fatigue, random fatigue, creep, and impact. In the present investigation, the durability of the tank is assessed using two load spectrums: static (gradual increase in internal pressure), and low cycle fatigue (pressurization/de-pressurization effect).

A total of fourteen failure criteria are computed in GENOA to determine ply failure. The first twelve criteria are associated with the negative and positive limits of the six ply stress components in the material directions 1 to 3. Those twelve criteria are stress limits calculated by the micromechanical equations based on material's constituent stiffness and strength values (Ref. 5). The computed modes of failures are: longitudinal tensile/compressive, transverse tensile/compressive, normal tensile/compressive; positive and negative in-plane shear, transverse normal shear, and longitudinal normal shear; modified distortion energy, and relative rotation. If ply damage is predicted due to longitudinal tensile or compressive failure, ply stiffness is reduced to zero at the damaged node. If ply damage is predicted due to transverse tensile, transverse compressive, or shear failures, only the matrix stiffness is degraded and the longitudinal stiffness of the fiber is retained. In the computation of the modified distortion energy the combined stresses are included as failure criteria. The relative rotation criterion considers failure if the adjacent plies rotate excessively with respect to one another (interply delamination). Analysis results are presented in the next two sections.

V. Stress and Displacement Analysis

Prior to discussing the results obtained from stress and displacement analysis, it is imperative to describe the composite tank loading scenario. At design conditions, the operating internal pressure for the LH2 composite tank is estimated at 30 psi. The results presented in this paper are based on the assumption that the composite and the liner have reached a steady state temperature equivalent to that of the propellant of -423 °F. As mentioned earlier in the paper, the weight of the tank and its LH2 fuel combined is estimated to be around 178,560 lb. Proper structural analysis must take into account the inertial (acceleration) loads. As shown in Fig. 3, the tank is subjected to a 3g load equivalent to 536 kips axially and 2.5g load acting in the normal direction and equivalent to 446 kips. The vector sum of these two inertia components is equivalent to 4g, which is a limit enforced on the trajectory analysis. This inertia loading is conservative, because some of the propellant would be burned before these loads are attained.

The stress analysis is performed using the aforementioned inertial loads and an internal pressure of 30 psi. The longitudinal, transverse, and shear stresses for all plies are evaluated at design internal pressure. The objective here is to ensure that the considered design configuration does not yield any ply damage or failure. The results obtained at design conditions are encouraging because none of the failure criterion evaluated through GENOA are active. The stresses for the composite ply that contains the aluminum liner are plotted in Fig. 3 (b through d). One can easily compare the ply stress magnitude to the ply strengths that are tabulated in Table 3. The results indicate that the maximum stress to strength ratio is about 0.77 (ratio of tensile ply transverse stress to ply transverse strength). Other stress components are far less than their correspondent strength limit. Although stress contour plots are shown for one ply in the paper, the durability analysis did not indicate any ply failure when the inertial loads and 30 psi internal pressure are applied.

Figure 4 shows the composite tanks global displacements in the three directions (X, Y, and Z). The displacement analysis was performed twice: (1) with internal pressure and inertial loads, and (2) with internal pressure only. The purpose of the two evaluations is to underline the importance of including the inertial loads. Note that the maximum growth in the tank (X displacement) is 1.7" when inertial loads are included in the analysis. The same displacement is 1.2" when inertial loads are not included in the analysis. But the effect of the inertial loads is obvious when one examines the displacements normal to the length of the tank in Y and Z directions. With the inertial loads, the Y displacement is close to 2" while it is 0.6" without the inertial loads. The center displacement (Z direction) is also 1.5" with inertial loads compared to 0.35" without inertial loads. Also note the change in the displacement mode (Y direction) when the inertial loads are considered. The tank undergoes compression type deformation (in the upper section), which is consistent with the physics of the problem. Information pertaining to the growth in the tank is crucial design data because it is used in determining how much clearance to allow. Deflection at the center of the composite tank is plotted versus the internal pressure load in Fig. 5. The intent here is to assess the effect of increased internal pressure on the deflection in the center of the composite tank while maintaining constant inertial loads. The plot in Fig. 5 indicates that the deflection becomes non-linear rapidly as soon as the tank is loaded. As the internal pressure is increased from about 10 psi to 160.5 psi, the deflection goes from 1.25" to 1.9". The trend in the displacement indicates that the structure is stable and the design is robust.

Since no ply failure has occured under design conditions, and since the displacements in the tank can be considered small in comparison to the tank size, the robustness of the design must be evaluated by damage progression analysis. Results from durability analysis are presented in the next section for static type loading and for cyclic loading as well. The inertial loads are included, as they should be, in the damage progression and durability analysis.

VI. Durability Analysis of LH2 Composite Tank

Prior to discussing the composite tank results from durability analysis, it is important to define some key parameters that are referenced in this section. Damage initiation load is defined as the load that causes one or more plies to fail. Damage propagation load is defined as the load that causes damage to propagate while the structure is stable (prior to reaching a critical stage). Ultimate load is defined as the final load that the structure can withstand before it bursts (catastrophic failure). Damage tolerance is defined as the additional damage that a structure can sustain from the point when damage is initiated until the ultimate load is reached. Damage (%) is defined as the percent ratio of total damage volume in the composite to total volume of composite structure. Damage energy is the energy used to create the damage. Damage energy release rate is defined as the ratio of incremental work done by external forces to the incremental volume of damage created during a load increment (i.e. damage energy divided by incremental damage volume). Further details pertaining to analytical damage progression methods in composite structures can be found in references 4, 5, and 6.

Durability analysis is performed using GENOA for static type loading, which increments the internal pressure while holding the temperature at –423°F along with the inertial loads. GENOA is also used to perform low cycle fatigue analysis to assess the effect of pressurization and de-pressurization on the damage in the composite tank.

A. Static Loading

The damage percent sustained as the internal pressure in the tank is increased is plotted in Fig. 6. The results show that the tank first ply failure occurs under an internal pressure of 54 psi. The damage initiation pressure is 1.8 times the design pressure of 30 psi. Note that the design specification states that the burst pressure shall be 1.5 times the 30 psi design pressure or 45 psi. As the pressure is increased, the damage increases from 0.4% at 54 psi to 34.5% at the ultimate pressure of 160.5 psi. The damage tolerance of the composite tank is estimated to be 106.5 psi.

The tank can tolerate additional 106 psi before it bursts. Most of the damage occurred when the internal pressure is increased from 61 to 85 psi, where the damage went from 4% to 30%. When the pressure is increased from 85 psi to 160.5 psi, the damage goes from 30 to 34.5%. The aluminum liner is damaged at an internal pressure of 72 psi. That is when leakage would start taking place. Therefore, the tank deems unusable as soon as the tank pressure reaches 72 psi. The solution option used in the analysis ignored the plasticity for the liner. Because the liner is inside the tank, the deformation for the liner is constrained by the outside composite layers. The plasticity will not occur until the composite layers are broken.

The damage energy expended at increased internal pressure is plotted in Fig 7. The damage energy is summed up over local damage volumes. The more damage volume there is, the higher the damage energy will be. As shown in Fig. 7, the damage energy rate (with respect to increases in the applied load) steadily increases when the pressure is between 54 and 160.5 psi. The rate of damage accumulation with respect to the increasing load is reduced as the internal pressure is increased beyond 85 psi. The structure it still able to sustain the pressure load (up to 160 psi) indicating that the structure is still durable. The damage energy release rate is plotted in Fig. 8 for increased pressure load. As mentioned earlier, the damage energy release rate is the change in the damage energy with respect to a change in the damaged volume. When the damage energy release rate peaks, and the damage energy is increasing with respect to the applied load, it implies that damage volumes are failing due to additional failure mechanisms. That is evident in the damage plots that are presented in Fig. 6, 7, and 8.

The damage initiation mechanism and related failure modes are described in Fig. 9. When the internal pressure reaches 54 psi, two ply failure modes are active: transverse tensile (matrix cracking) and relative rotation (interply delamination). Initial damage occurs because 4 plies have failed as depicted in Fig. 9. The damage progression history is presented in Fig. 10 and 11 for the internal pressure loads: 54, 61.5, and 160.5 psi. The 61.5 psi pressure is considered the damage propagation load (damage volume is 4%). When the ultimate load of 106.5 psi is reached, the additional failure modes that become active are: longitudinal tensile, in-plane shear, and modified distortion energy (combined stress). The ply failure summary and progression history presented in Fig. 9, 10, and 11 provided an unprecedented ability to detect when damage takes place, and why damage takes place and how to prevent damage from taking place. The computational simulation process employed in this evaluation is similar to an "on-line virtual laboratory ". Damage initiation cannot be detected in a laboratory setting unless fracture takes place. Therefore, it is highly recommended to make use of available computational technology to reduce the cost of expensive testing.

B. Low Cycle Fatigue Analysis

The results presented in the previous section demonstrated the robustness of the stiffened design concept. But in order for the structural component to be re-usable, one must perform low cycle fatigue analysis to ensure that the pressurization and de-pressurization process of the tank does not pose any threat to the integrity and safety of the vehicle. As a result, GENOA is used to determine how many cycles it would take to initiate damage in the tank and how many cycles can the structure sustain before any failure takes place. In GENOA, low cycle fatigue loading is applied as a static loading. Prior to performing low cycle fatigue analysis, one must define a set of parameters that pertains to cyclic degradation factors for the fiber and matrix. Equation (3) defines the fiber or matrix degradation factor:

$$\text{Degradation factor for fiber} = a_f - b_f \log(N) \qquad (3\text{-a})$$

$$\text{Degradation factor for matrix} = a_m - b_m \log(N) \qquad (3\text{-a})$$

Where N is the number of cycles, and the parameters a and b are used to degrade the fiber or matrix properties. The analysis results presented in this section are obtained based on value of 1.0 for a and a value of 0.2 for b. Traditionally, these degradation parameters are predicted with experimental methods or through available/documented test data. Additional details on this subject can be found in Ref. 4.

The analysis performed is based on an internal design pressure of 30, cryogenic structural temperature, and application of inertial loads as seen in previous sections. The damage percent sustained as the tank is filled and emptied is plotted in Fig. 12 versus the number of cycles. Damage initiates in the structure as soon as the number of cycles reaches 100 (0.075% damage). The damage increases monotonically with the number of cycles. At 500 cycles, 5% of the structure is damaged, the liner is damaged at 600 cycles, and at 1000 cycles 21% of the structure is damaged. The correspondent damage energy is plotted in Fig 13. Note that damage energy is low when the damage is low. That is manifested in Fig 14 where the damage energy is low up to 500 cycles and it increases rapidly as the damage volume is increased from 5% at 500 cycles to 21% at 1000 cycles. The characteristics of the damage phenomenon are also evident in the damage energy release rate plot shown in Fig. 14. The plot shows a reduction in the stability of the tank as soon as the number of cycles reaches 500. The damage energy release rates drops sharply

after 500 cycles indicating that additional failure modes have become active. The damage progression history due to cyclic loading is presented in Fig. 15. When damage initiates, the failure modes that are active are similar to those under static type loading but occur at different locations in the tank. After 1000 cycles, the damage spreads to the body of the tank but no fracture has taken place indicating that the design concept, once again, is robust and effective. The damage mainly is concentrated in the upper region and rear cap of the tank. The upper section of the tank is under compression due to the inertial loads. The damage results are consistent with the physics resulting from the load application.

VII. Conclusion

A formal computational method that combines finite element structural analysis with composite mechanics and progressive fracture is an effective tool for evaluating advanced design concepts in cryogenic tank applications. Results from the investigative study of the internally stiffened LH2 composite tank are: (1) a safety factor of 1.8 (54 psi for damage initiation) can be achieved without a large increase in the weight of the tank, (2) the usability of tank is sustained up to an internal pressure that is nearly 2.5 times the 30 psi design pressure, and (3) a hundred cycles can be attained by the proposed design. Future computational work should account for the effect of thermal gradient through the tank skin. A detailed thermal analysis of the entire flight vehicle is needed to properly predict the thermal loads. Based on the success of this evaluation, one can perform comparable evaluations on other cryogenic tanks. The simulation presented in the paper can serve as an effective guide prior to and during a test program. Material testing is recommended to verify the liner and laminate properties at cryogenic temperatures. It is also recommended that one verifies existing models for degrading material properties under cyclic loading conditions. Furthermore, future efforts must quantify the effect of uncertainty in the fiber and matrix material properties, loading, service environment, and fabrication process on the structural performance of the tank.

References

[1]Abdi, F. and Su, X., "Composite Tank Permeation and Crack Density Prediction and Verification", ASME Symposium on Space Applications of Composites, Washington, DC, 2003.

[2]Greenberg, H.S., "Milestone 10-Test Report of Composite Tank Material Screening Tests", Rockwell Aerospace Report, 1995.

[3]Johnson, T.F. and Gates, T.S., "Temperature Polyamide Materials in Extreme Temperature Environment", 42nd AIAA/ASME/ASCE/AHS/ASC Structural Dynamics and Materials Conference, Seattle, WA, 2001.

[4]GENOA, Progressive Failure Analysis for 2D/3D Laminate/Woven/Braided/Stitched Polymer and Ceramic Matrix Composite, Software Package, Ver. 3.2, Alpha Star Corporation, Long Beach, CA, 2004.

[5] Murthy, P.L.N. and Chamis, C.C, "ICAN: Integrated Composites Analyzer," *Journal of Composites Technology & Research*, 1986,Vol. 24, No. 11, pp. 1872-1873.

[6]Minnetyan, L., Chamis, C.C., and Abdi, F., "Damage Tolerance of Fiber Composite Airfoils with Piezoelectric Adaptive Control System", AIAA 2000-1504, 2000.

Table 1: Properties of IM7 Fiber/977-2 Matrix at Cryogenic Temperature of -423 °F

Fiber IM7			**Matrix 977-2**		
Weight density	6.312E-02	lb/in^3	Weight density	0.457E-01	lb/in^3
Normal modulus (11)	4.000E+07	psi	Normal modulus	1.600E+06	psi
Normal modulus (22)	2.100E+06	psi	Poisson's ratio	0.48	
Poisson's ratio (12)	0.22		Thermal expansion coef.	0.600E-05	in/in/°F
Poisson's ratio (23)	0.200		Matrix tensile strength	9.900E+03	psi
Shear modulus (12)	2.000E+06	psi	Matrix compressive strength	33.50E+03	psi
Shear modulus (23)	8.500E+05	psi	Matrix shear strength	2.170E+04	psi
Thermal expansion coef. (11)	1.500E-07	in/in/°F			
Thermal expansion coef. (22)	3.000E-06	in/in/°F			
Fiber tensile strength	6.590E+05	psi			
Fiber compressive strength	3.550E+05	psi			

Table 2: Ply Schedule Details for the Stiffened LH2 Tank

Ply Schedule	Fiber	Matrix	Fiber Volume Ratio	Ply Layup	Ply Thickness	Liner Thickness Aluminum 6061
1	IM77	977-2	0.6	$[+/- 75,0,90,0]_s$	0.01"	0.005"
2	IM77	977-2	0.6	$[+/- 75,0,90,0]_{2s}$	0.01"	0.005"
3	IM77	977-2	0.65	$[0,90,0,90,0]_s$	0.01"	0.005"

Table 3: IM7/977-2 Composite Properties at Cryogenic Temperature of -423 °F

Property	Fiber Volume Ratio:	0.60	0.65
Elastic Modulus $_{(11)}$ (psi)		2.46E+07	2.66E+07
Elastic Modulus $_{(22)}$ (psi)		1.96E+06	1.98E+06
Elastic Modulus $_{(33)}$ (psi)		1.96E+06	1.98E+06
Shear Modulus $_{(12)}$ (psi)		1.97E+06	2.21E+06
Shear Modulus $_{(23)}$ (psi)		6.92E+05	7.08E+05
Shear Modulus $_{(13)}$ (psi)		1.97E+06	2.21E+06
Poisson's Ratio $_{(12)}$		0.32	0.31
Poisson's Ratio $_{(23)}$		0.49	0.46
Poisson's Ratio $_{(13)}$		0.32	0.31
Thermal Expansion Coefficient $_{(11)}$ (in/in/°F)		3.02E-07	2.73E-07
Thermal Expansion Coefficient $_{(22)}$ (in/in/°F)		4.31E-06	4.13E-06
Thermal Expansion Coefficient $_{(33)}$ (in/in/°F)		4.31E-06	4.13E-06
Density (lb/in^3)		0.056	0.057
Longitudinal Tensile Strength (psi)		395,400	428,300
Longitudinal Compressive Strength (psi)		206,300	210,000
Transverse Tensile Strength (psi)		9,488	9,532
Transverse Compressive Strength (psi)		32,110	32,250
Shear Strength (psi)		18,150	18,530

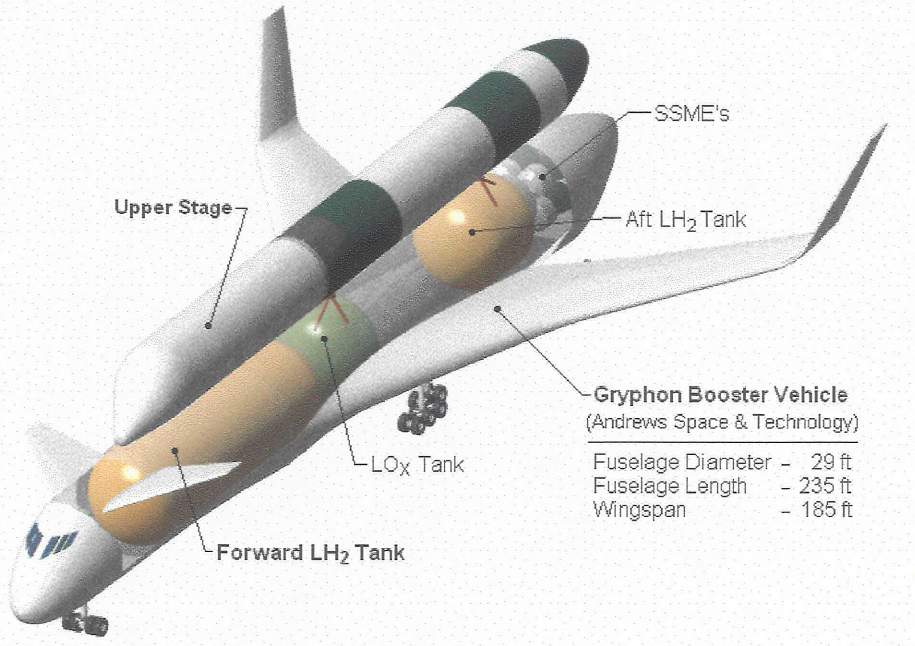

Figure 1: Schematic of the Andrews Space Gryphon Vehicle

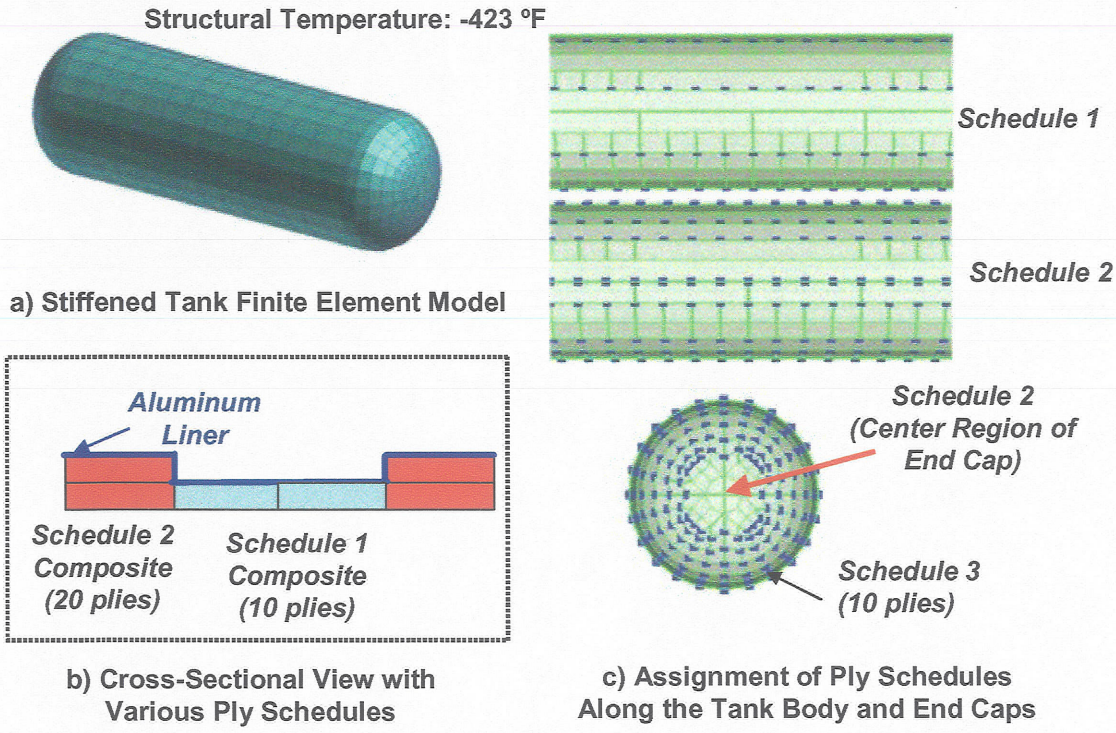

Figure 2: Stiffened LH2 Tank Finite Element Model and Assignment of Ply Schedules

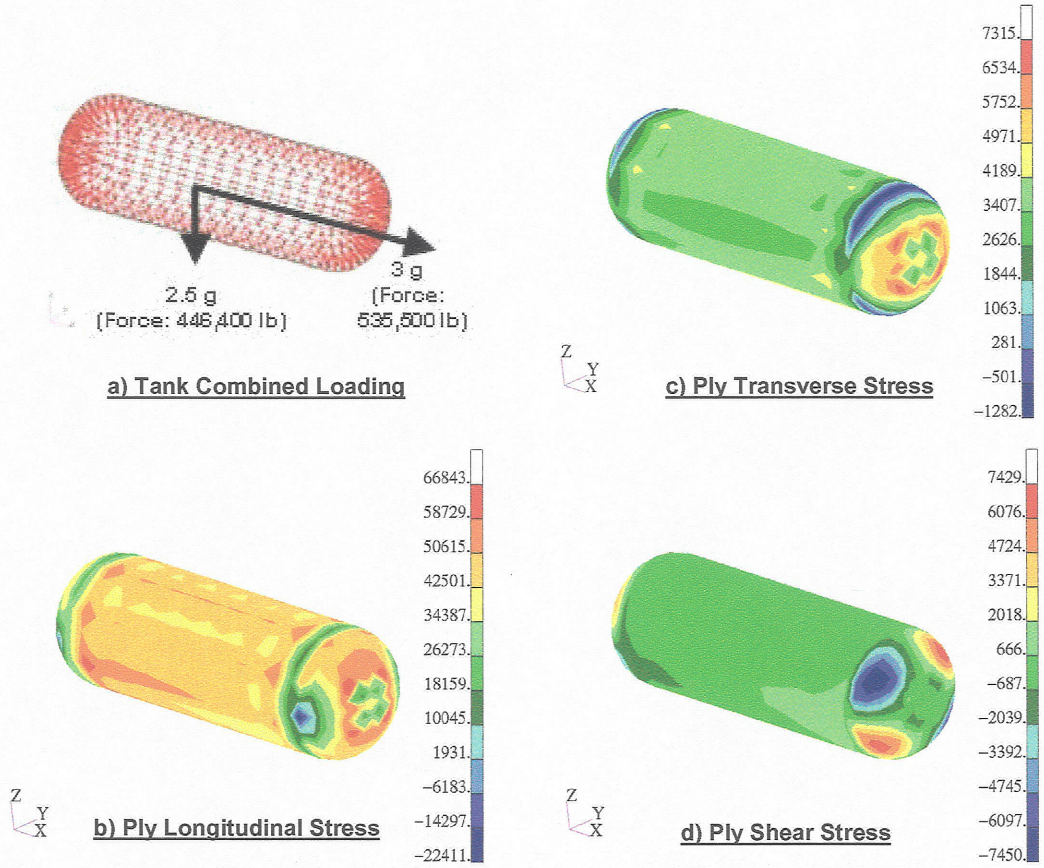

Figure 3: Stresses in the First Composite Ply which Contains the Aluminum Liner (Structure Evaluated at a Temperature of -423 °F and an Internal Pressure of 30 psi)

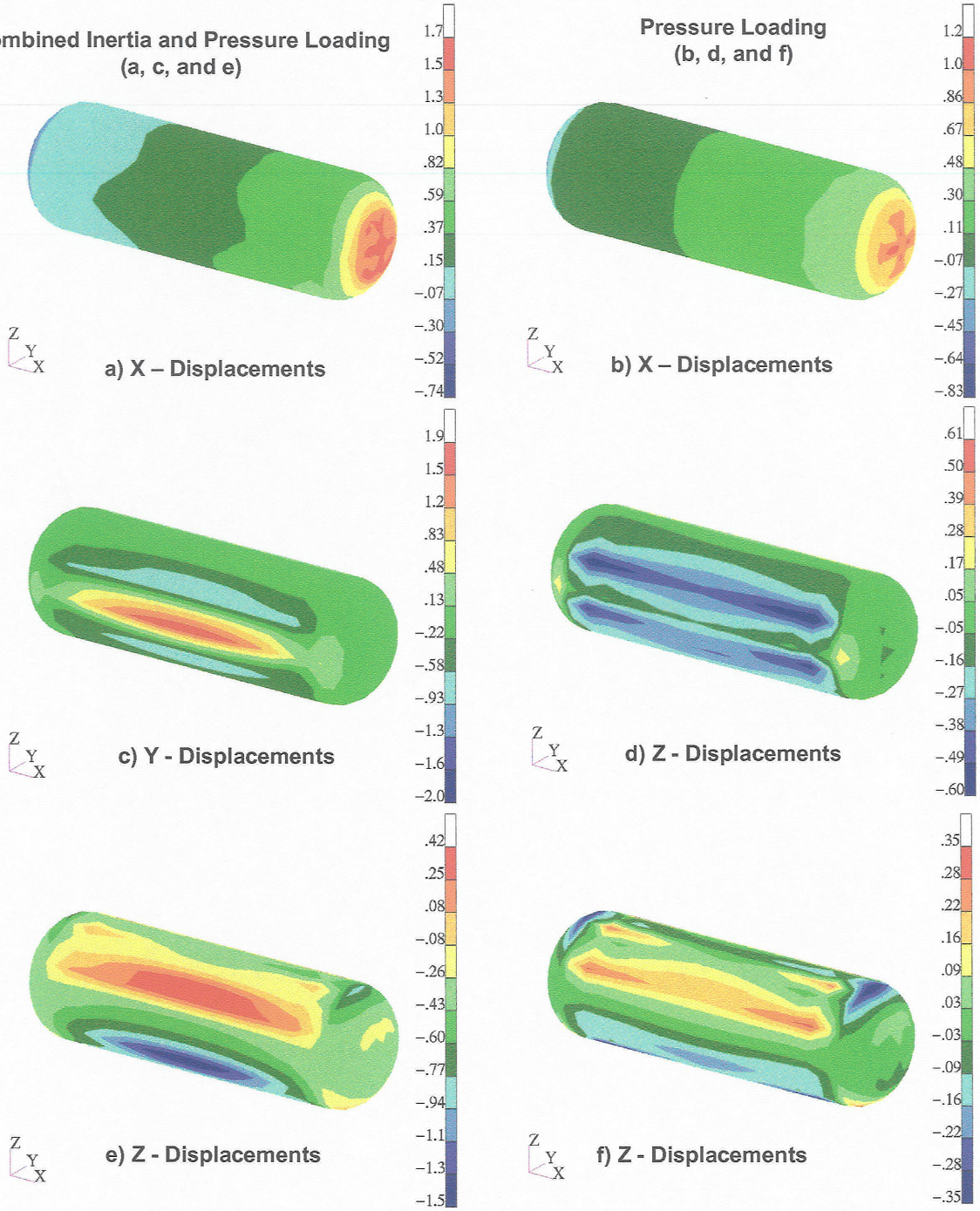

Figure 4: Composite Tank Displacements Under Design Internal Pressure of 30 psi (With and Without Inertial Loads Based on -423 °F Structural Temperature)

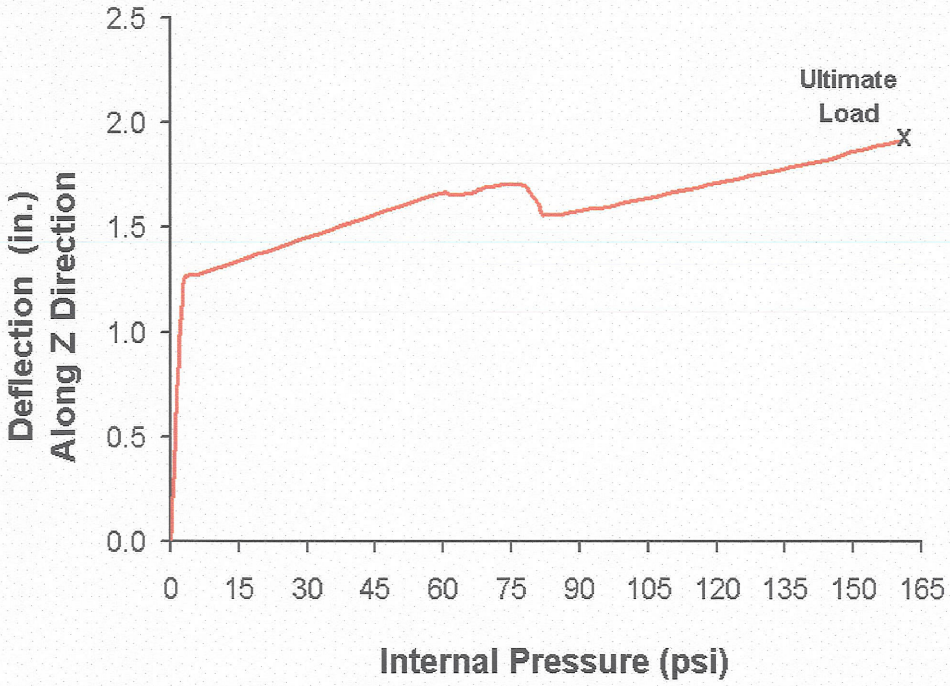

Figure 5: Deflection in the Center of the Tank as a Function of Increased Internal Pressure (Structure Evaluated at a Temperature of -423 °F)

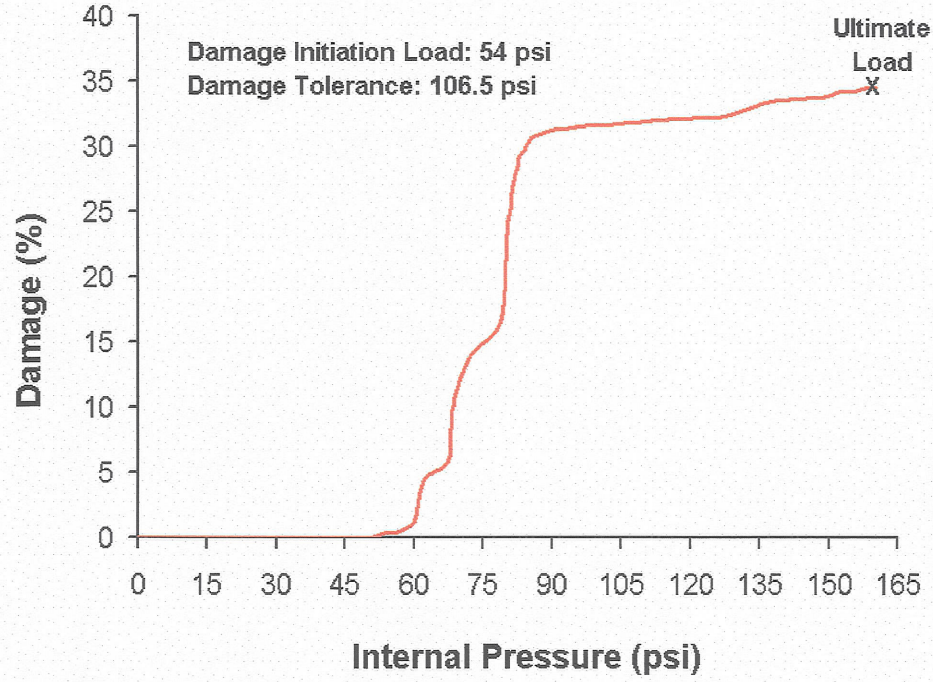

Figure 6: Damage Sustained (%) as a Result of Increased Internal Pressure (Structure Evaluated at a Temperature of -423 °F)

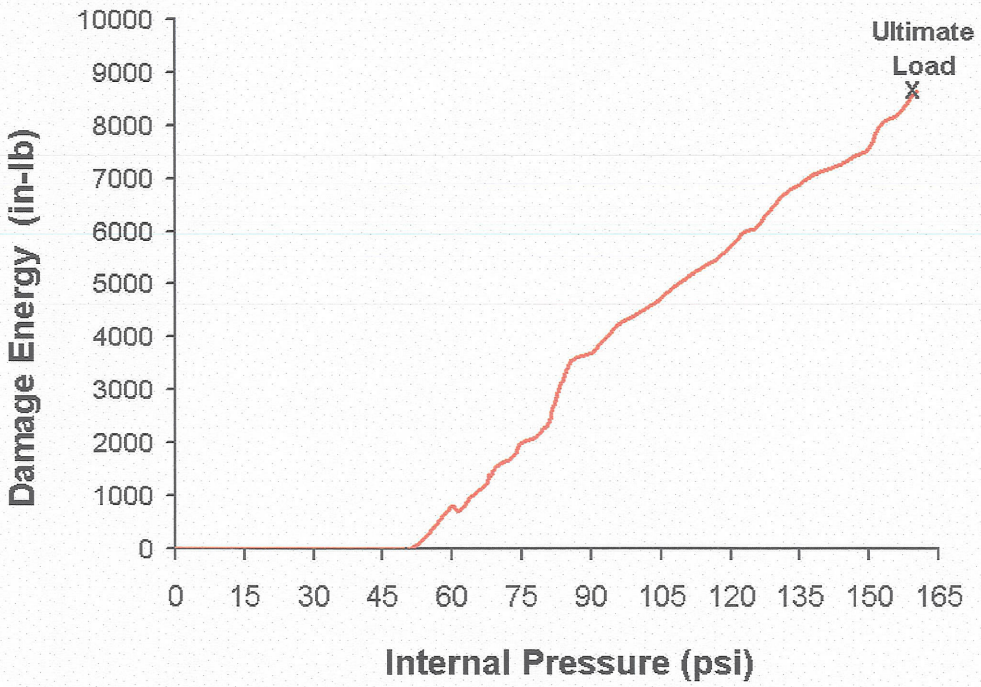

Figure 7: Damage Energy Produced as a Result of Increased Internal Pressure (Structure Evaluated at a Temperature of -423 °F)

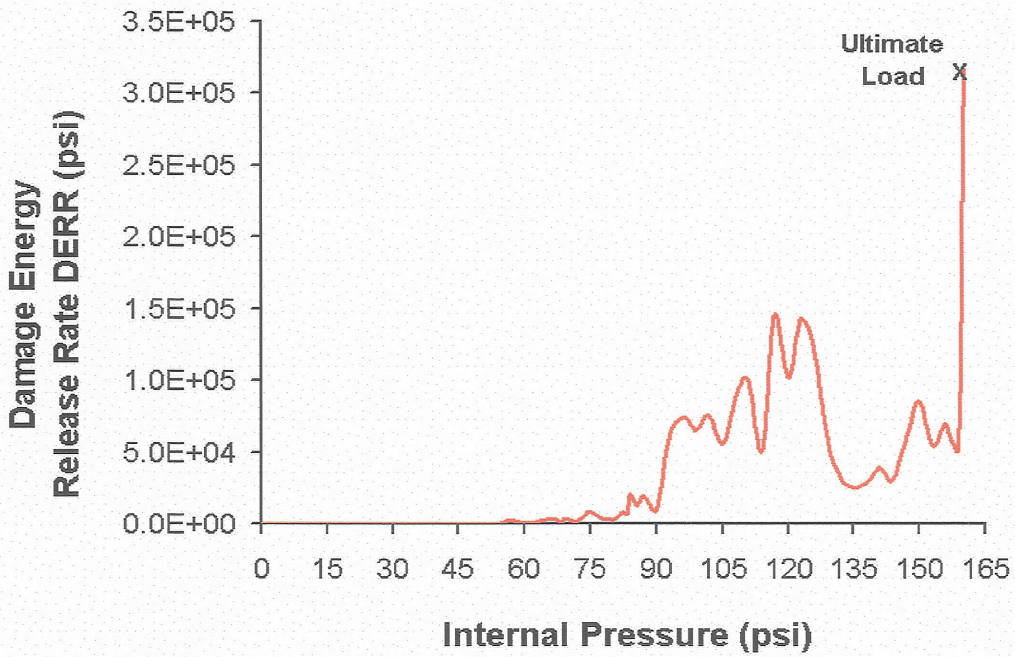

Figure 8: Damage Energy Release Rate as a Result of Increased Internal Pressure (Structure Evaluated at a Temperature of -423 °F)

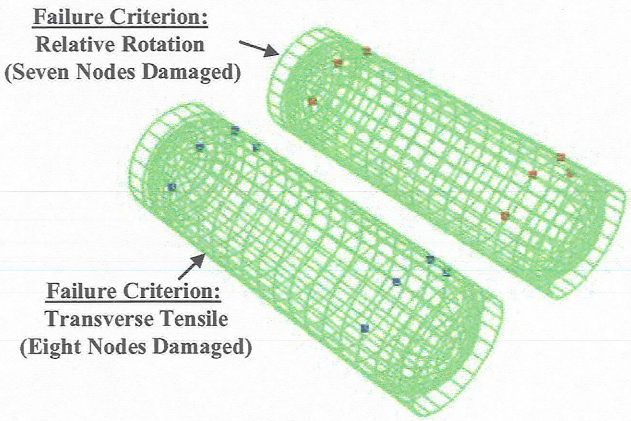

Ply Number	Material Type	Orientation (Degrees)	Thickness (in.)
1	IM7/977-2	75	0.01
2	IM7/977-2	-75	0.01
3[1,2]	IM7/977-2	0	0.01
4	IM7/977-2	90	0.01
5[1,2]	IM7/977-2	0	0.01
6[1]	IM7/977-2	0	0.01
7	IM7/977-2	90	0.01
8[1,2]	IM7/977-2	0	0.01
9	IM7/977-2	-75	0.01
10	IM7/977-2	75	0.01
11	Aluminum		0.005

Ply Failed: [1] Transverse Tensile , [2] Relative Rotation

Figure 9: Damage Initiation in the LH2 Tank Under an Internal Pressure of 54 psi (Structure Evaluated at a Temperature of -423 °F)

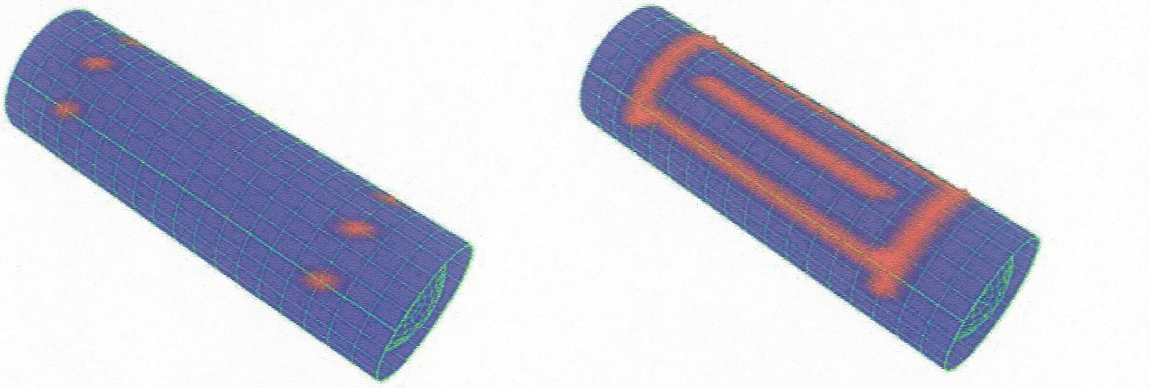

a) Damage Initiation (54 psi Pressure) Damage Volume: 0.4%

b) Damage Propagation (61.5 psi Pressure) Damage Volume: 4%

Figure 10: Damage Propagation at Increased Internal Pressure (Structure Evaluated at a Temperature of -423 °F)

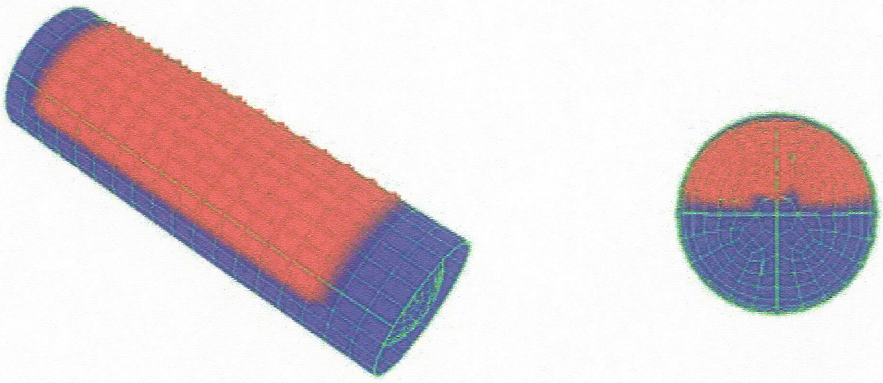

a) 3-D View Damage Prior to Burst Damage Volume: 34.5%

b) 2-D View Damage Prior to Burst Damage Volume: 34.5%

Figure 11: Damage in the Tank Under an Ultimate Pressure of 160.5 psi (Structure Evaluated at a Temperature of -423 °F)

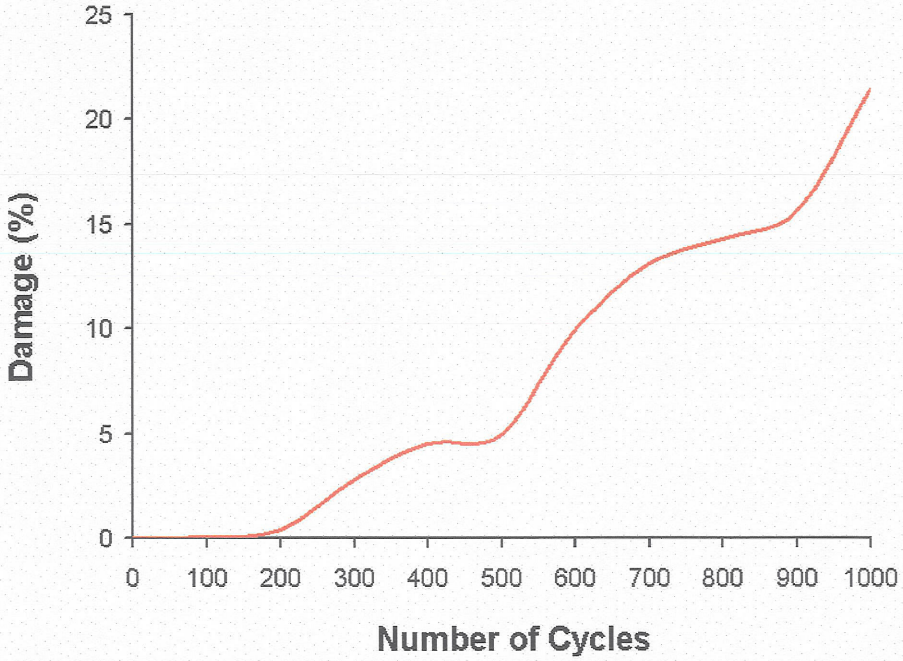

Figure 12. Damage Sustained (%) Under Cyclic Loading (Pressurization and De-Pressurization) (Structure Evaluated at a Temperature of -423 °F and an Internal Pressure of 30 psi)

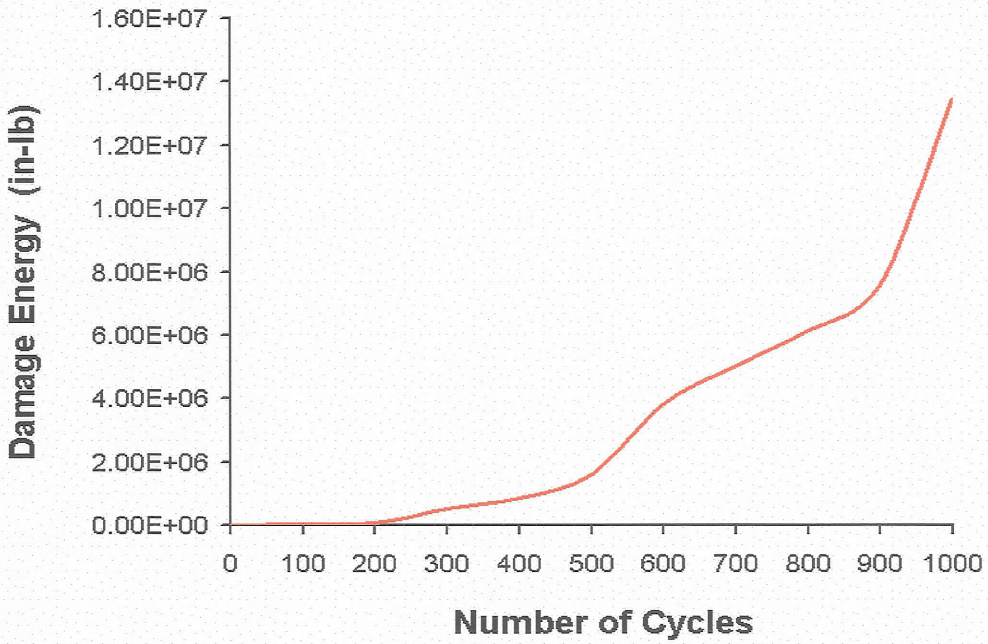

Figure 13. Damage Energy Produced Under Cyclic Loading (Pressurization and De-Pressurization) (Structure Evaluated at a Temperature of -423 °F and an Internal Pressure of 30 psi)

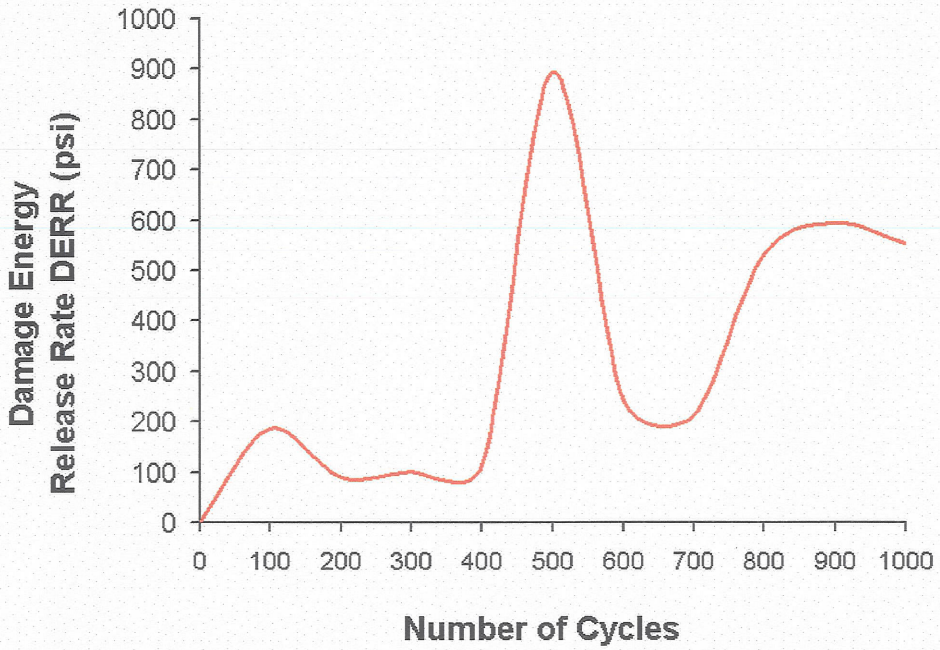

Figure 14: Damage Energy Release Rate Under Cyclic Loading (Pressurization and De-Pressurization (Structure Evaluated at a Temperature of -423 °F and an Internal Pressure of 30 psi)

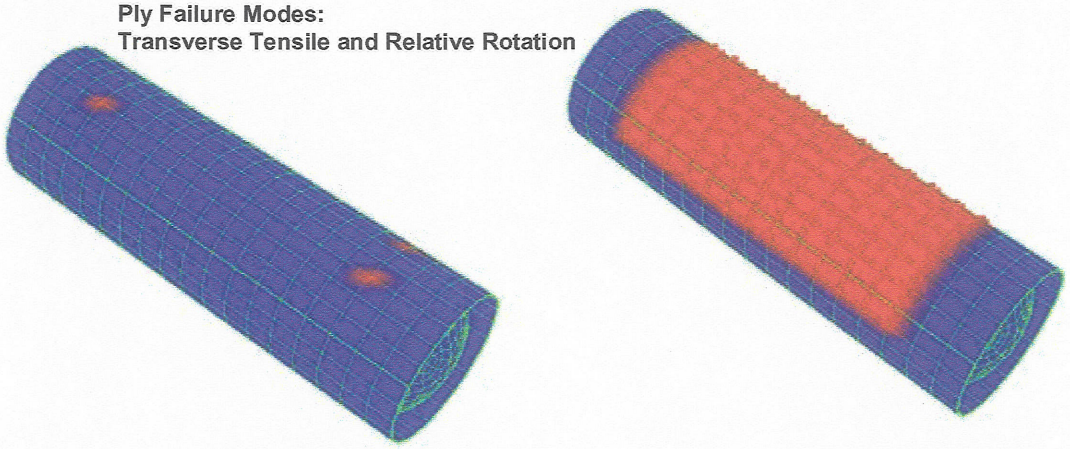

a) Damage Initiation (100 Cycles)
Damage Volume: 0.075%

b) Damage Propagation (1000 Cycles)
Damage Volume: 21.4%

Figure 15: Damage Initiation and Propagation in the LH2 Tank Under Cyclic Loading (Structure Evaluated at a Temperature of -423 °F and an Internal Pressure of 30 psi)